Computational Mechanics 33 (2004) 263–273 © Springer-Verlag 2003
DOI 10.1007/s00466-003-0527-z

Analysis of cylindrical bending thermoelastic deformations of functionally graded plates by a meshless local Petrov–Galerkin method

L. F. Qian, R. C. Batra, L. M. Chen

Abstract We analyze plane strain static thermoelastic deformations of a simply supported functionally graded (FG) plate by a meshless local Petrov–Galerkin (MLPG) method. Material moduli are assumed to vary only in the thickness direction. The plate material is made of two isotropic randomly distributed constituents and the macroscopic response is also modeled as isotropic. Displacements and stresses computed with the MLPG method are found to agree very well with those obtained from the analytical solution of the problem. The number of nodes required to obtain an accurate solution for a FG plate is considerably more than that needed for a homogeneous plate.

Keywords Plane strain deformations, Thermoelasticity, Meshless method, Inhomogeneous material

1 Introduction

Functionally graded materials (FGMs) permit tailoring of material properties so as to derive maximum benefits from its inhomogeneity. FGMs have been used for structural optimization (bamboo is a highly optimized naturally occuring FGM) [25], increasing electric conductivity without impairing the thermal insulation of ceramics [28], enhancing biocompatibility [39], devising new power generation techniques [44], reducing thermal stresses [36], and relieving stress intensity factors due to a thermal shock [17]. An advantage of an FGM over laminated composites is that material properties vary continuously through the thickness rather than being discontinuous across adjoining layers thereby mitigating the delamination mode of failure. However, in an FGM made of particulates, failure may occur due to decohesion at the particulate/matrix interfaces.

A theoretical framework to analyze and design FG structures needs (i) the relationship between the microstructures and the macroscopic response, and (ii) analytical/numerical tools to analyse inhomogeneous structures. Techniques to ascertain the effective elastic moduli of an FGM include the three-phase model [11], the Mori–Tanaka method [24], the self-consistent technique [14], a higher-order unit cell method [1], a fuzzy logic method [15], the mean field theory [16], the representative volume element technique and the rule of mixtures. Vel and Batra [40, 43] have given analytical solutions for thermomechanical deformations of simply supported FG plates subjected to either time-independent thermal and mechanical loads or transient thermal loads. They [41] have also analyzed natural frequencies of a simply supported FG plate. The method of asymptotic expansions has been used by Rogers et al. [34], Tarn and Wang [38] and Cheng and Batra [7] for studying deformations of a simply supported FG plate. One could also use the finite element method (FEM) or a meshless method. Meshless methods such as the element-free Galerkin [6], the hp-clouds [10], the reproducing kernel particle [21], the smooth particle hydrodynamics [22], the diffuse element [26], the partition of unity finite element [23], the natural element [37], meshless Galerkin methods using radial basis functions [45], and the meshless local Petrov–Galerkin (MLPG) [2] for finding an approximate solution of a given initial-boundary-value problem have become popular because nodes can be placed at arbitrary locations. The finite-difference method and the collocation technique are also meshless methods of finding an approximate solution of a given boundary-value problem. These methods and other developments on meshless methods are discussed in two recent books [3, 20].

Advantages of the MLPG method are that it employs a weak formulation of the problem and no background mesh is required to numerically evaluate various integrals appearing in the local Petrov–Galerkin formulation of the problem. However, a higher-order integration rule is generally needed to evaluate these integrals. Ching and Batra [9] used the MLPG method to ascertain singular fields near a crack tip by enriching the basis functions and employing either the visibility [6] or the diffraction criterion [27]. The MLPG method has also been successfully used to study 2-dimensional elastodynamic problems for

Received: 26 June 2003 / Accepted: 27 October 2003
Published online: 15 December 2003

L. F. Qian, L. M. Chen
Nanjing University of Science and Technology
Nanjing 210094, P. R. China

R. C. Batra (✉)
Department of Engineering Science and Mechanics,
M/C 0219 Virginia Polytechnic Institute and State University
Blacksburg, VA 24061, USA
e-mail: rbatra@vt.edu

The work was partially supported by the Office of Naval Research grant N00014-98-1-0300 to Virginia Polytechnic Institute and State University with Dr. Y. D. S. Rajapakse as the program manager. L. F. Qian was also supported by the China Scholarship Council.

homogeneous bodies [12, 4]. Qian, Batra and Chen [29–31] have used the MLPG method in conjunction with a higher-order shear and normal deformable plate theory (HOSNDPT) [46] to analyze static and dynamic deformations of a homogeneous and a functionally graded plate. It was found that results could satisfactorily be computed even when Poisson's ratio for the plate material equaled 0.499. Qian and Batra [32, 33] have used the compatible HOSNDPT and the MLPG method to analyse transient heat conduction and transient thermoelastic deformations in a FG plate. Batra, Porfiri and Spinello [5] have used the MLPG method to study transient heat conduction in a bimetallic disk; the discontinuity in the temperature gradient at the common interface is satisfied by using either the method of Lagrange multipliers or by employing the jump function proposed by Krongauz and Belytschko [18]. We use the MLPG method here to analyze plane strain static thermoelastic deformations of an FG plate with material properties varying smoothly in the thickness direction. Whereas Qian and Batra [33] used a compatible HOSNDPT to analyse three-dimensional deformations of a plate, we employ here the two-dimensional thermoelasticity equations and analyse static plane strain deformations. With material properties varying only in the thickness direction, the partial differential equations of the plate theory have constant coefficients for a plate of uniform thickness. However, for the plane strain problem, the coefficients in the partial differential equations are functions of the thickness coordinate. The present work is a better test of the applicability of the MLPG method for analysing deformations of an inhomogeneous body than that presented in [31].

The paper is organized as follows. Section 2 gives the formulation of the problem, and Sect. 3 describes briefly the MLPG method and its implementation for a thermoelastic problem. Computed results for an Aluminum/Silicon Carbide FG plate are compared with the analytical solution in Sect. 4. Section 5 summarizes conclusions.

2 Formulation of the problem

2.1 Governing equations

A schematic sketch of the problem studied and the rectangular Cartesian coordinate axes x_1, x_2, x_3 used to describe deformations of the FG plate are shown in Fig. 1. It is assumed that the plate occupies the region $\Omega = [0, L] \times [-h/2, h/2] \times (-\infty, \infty)$ in the unstressed reference configuration. The cross-section of the plate is denoted by $S = [0, L] \times [-h/2, h/2]$, and the boundary of S by Γ. The plate is made of an isotropic material with material properties varying only in the thickness (x_2) direction.

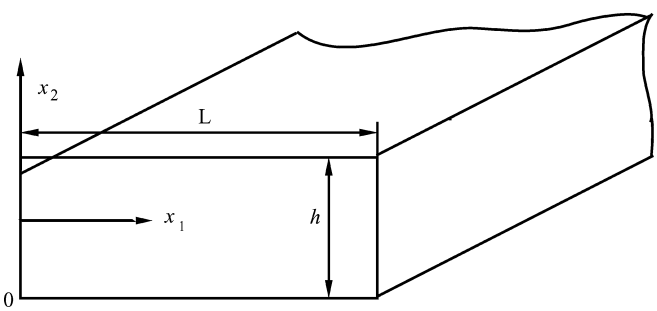

Fig. 1. Schematic sketch of the problem studied

In the absence of body forces and sources of internal energy, static thermoelastic deformations of an isotropic plate are governed by

$$\sigma_{ij,j} = 0, \quad q_{i,i} = 0, \quad \text{in} \quad \Omega, \quad i,j = 1,2,3 \ , \tag{1}$$

$$\sigma_{ij} = \lambda \varepsilon_{kk} \delta_{ij} + 2\mu \varepsilon_{ij} - \beta \delta_{ij} T, \quad q_j = -\kappa T_{,j}, \quad \text{in } \Omega \ , \tag{2}$$

$$\varepsilon_{ij} = (u_{i,j} + u_{j,i})/2, \quad \text{in } \Omega \ . \tag{3}$$

Here $\boldsymbol{\sigma}$ is the stress tensor, $\mathbf{q}$ the heat flux, $\boldsymbol{\varepsilon}$ the infinitesimal strain tensor, $\mathbf{u}$ the displacement, T the change in temperature from that in the stress-free reference configuration, a comma followed by j indicates partial differentiation with respect to x_j, a repeated index implies summation over the range of the index, $\mathbf{x}$ gives the position of a material particle, $\boldsymbol{\delta}$ is the Kronecker delta, λ and μ are Lamé constants, $\beta = 3K\alpha$ is the stress-temperature coefficient, K is the bulk modulus, α is the coefficient of thermal expansion, and κ is the thermal conductivity. Material parameters λ, μ, β and κ are smooth functions of x_2. Equation $(1)_1$ expresses the balance of linear momentum, and Eq. $(1)_2$ the balance of internal energy. Equation $(2)_1$ is Hooke's law and Eq. $(2)_2$ the Fourier law of heat conduction.

We assume that a plane strain state of deformation prevails in the plate, and boundary conditions and thermomechanical loads applied to it are independent of the x_3-coordinate. Thus $u_3 = 0$, and u_1, u_2 and T are independent of x_3. Henceforth indices i and j take values 1 and 2. Boundary conditions considered are

$$\begin{aligned} &\sigma_{ij} n_j = f_i^{\pm}(x_1), \\ &q_i n_i = h^{\pm}(x_1) \quad \text{on } x_2 = \pm h/2, \\ &u_2 = 0, \\ &\sigma_{11} = 0, \\ &T = T_0 \quad \text{on } x_1 = 0, L \ . \end{aligned} \tag{4}$$

Here $\mathbf{n}$ is an outward unit normal to a surface, $\mathbf{f}^{\pm}$ the prescribed tractions and $h^{\pm}$ the prescribed heat flux on the top ($x_2 = h/2$) and the bottom ($x_2 = -h/2$) surfaces of the plate. Boundary conditions $(4)_{3,4}$ imply that the edges $x_1 = 0$ and $x_1 = L$ of the plate are simply supported; these do not simulate well conditions encountered in the laboratory where rollers or sharp edges are used to support a plate. However, these boundary conditions facilitate the comparison of the computed solution with the analytical solution [42]. Other types of boundary conditions can also be easily considered.

Substitution from (2) and (3) into (1) yields field equations for the displacement $\mathbf{u}$ and the temperature T.

These equations are one-way coupled in the sense that the field equation for T does not involve $\mathbf{u}$ but that for $\mathbf{u}$ involves T. Thus the temperature field can be found first, and then displacements can be computed.

2.2
Local weak formulation of the problem

Let $S_\alpha \subset S$ be a smooth closed region, and $\mathbf{v}$ and θ smooth functions defined on S_α. Let $\Gamma_{\alpha u}$, $\Gamma_{\alpha f}$, $\Gamma_{\alpha q}$ and $\Gamma_{\alpha t}$ denote parts of the boundary ∂S_α of S_α where displacements, surface tractions, heat flux and temperature are prescribed respectively. Note that $\Gamma_{\alpha u}$ and $\Gamma_{\alpha f}$ need not be disjoint since linearly independent components of the displacement and the surface traction may be prescribed at the same point of the boundary; e.g. see boundary conditions $(4)_3$ and $(4)_4$. However, for the sake of simplicity, $\Gamma_{\alpha u}$ and $\Gamma_{\alpha f}$ will be treated as disjoint parts of the boundary ∂S_α in this section. Let $\mathbf{u} = \bar{\mathbf{u}}$ and $T = \bar{T}$ be prescribed on $\Gamma_{\alpha u}$ and $\Gamma_{\alpha t}$ respectively, and $\sigma_{ij} n_j = \bar{f}_i$ and $q_i n_i = \bar{q}$ on $\Gamma_{\alpha f}$ and $\Gamma_{\alpha q}$ respectively. One way to impose essential boundary conditions (i.e. prescribed displacement $\bar{\mathbf{u}}$ on $\Gamma_{\alpha u}$ and prescribed temperature $\bar{T}$ on $\Gamma_{\alpha t}$) is to use the penalty method; another technique will be discussed in Sect. 3.4.

Let $\mathbf{v}$ and θ be smooth functions defined on S_α. Taking the inner product of Eq. $(1)_1$ with $\mathbf{v}$, of $(1)_2$ with θ, integrating the resulting equations on S_α, and using the divergence theorem, we arrive at

$$\begin{aligned}
&\int_{S_\alpha} v_{i,j}\sigma_{ij}\,\mathrm{d}A - \int_{\Gamma_{\alpha f}} v_i\bar{f}_i\,\mathrm{d}\Gamma \\
&\quad - \int_{\Gamma_{\alpha u}} v_i\sigma_{ij}n_j\,\mathrm{d}\Gamma + \int_{\Gamma_{\alpha u}} p_{iu}v_i(u_i - \bar{u}_i)\,\mathrm{d}\Gamma = 0, \\
&\int_{S_\alpha} \theta_{,i}q_i\,\mathrm{d}A - \int_{\Gamma_{\alpha q}} \theta\bar{q}\,\mathrm{d}\Gamma \\
&\quad - \int_{\Gamma_{\alpha t}} \theta q_i n_i\,\mathrm{d}\Gamma + \int_{\Gamma_{\alpha t}} p_t\theta(T - \bar{T})\,\mathrm{d}\Gamma = 0 \ .
\end{aligned} \tag{5}$$

Here p_{iu} and p_t are penalty functions defined on $\Gamma_{\alpha u}$ and $\Gamma_{\alpha t}$ respectively; p_{iu} assumes values much larger than those of λ, μ and β, and values of p_t are much greater than those of κ. In practice, p_{iu} and p_t are generally taken to be constants. The dimension of p_{iu} is stress/length, and that of p_t is thermal conductivity/length. In the 4th term on the left-hand side of Eq. $(5)_1$, the index i is summed even though it appears three times.

3
Meshless local Petrov–Galerkin (MLPG) formulation of the problem

Let M nodes be placed on S, and $S_1, S_2, \ldots, S_M$ be smooth two dimensional closed regions, not necessarily disjoint and of the same shape and size, enclosing nodes $1, 2, \ldots, M$ respectively, such that the union of $S_1, S_2, \ldots, S_M$ covers S. Let $\phi_1, \phi_2, \ldots, \phi_N$ and $\psi_1, \psi_2, \ldots, \psi_N$ with $N \le M$ be two sets of linearly independent functions defined on one of these regions, say S_I, $1 \le I \le N$. We approximate $\mathbf{u}$, $\mathbf{v}$, T and θ on S_I by

$$\begin{aligned}
\mathbf{u}(x_1, x_2) &= \begin{Bmatrix} u_1(x_1, x_2) \\ u_2(x_1, x_2) \end{Bmatrix} \\
&= \begin{Bmatrix} \sum_{J=1}^{N} \phi_J(x_1, x_2)\delta_J^1 \\ \sum_{J=1}^{N} \phi_J(x_1, x_2)\delta_J^2 \end{Bmatrix} \\
&= \{\phi^u\}^T\{\delta^u\}, \\
\mathbf{v}(x_1, x_2) &= \{\psi^u\}^T\{\bar{\delta}^u\}, \\
T(x_1, x_2) &= \{\phi^t\}^T\{\delta^t\}, \\
\theta(x_1, x_2) &= \{\psi^t\}^T\{\bar{\delta}^t\} \ .
\end{aligned} \tag{6}$$

The length of array $\{\delta^u\}$ is $2N$, and that of array $\{\delta^t\}$ is N. Substitution from $(6)_1$ into $(3)_4$ yields

$$\begin{aligned}
\boldsymbol{\varepsilon}(x_1, x_2) &= \begin{Bmatrix} \varepsilon_{11}(x_1, x_2) \\ \varepsilon_{22}(x_1, x_2) \\ 2\varepsilon_{12}(x_1, x_2) \end{Bmatrix} \\
&= \begin{Bmatrix} \sum_{J=1}^{N} \phi_{J,1}\delta_J^1 \\ \sum_{J=1}^{N} \phi_{J,2}\delta_J^2 \\ \sum_{J=1}^{N} (\phi_{J,2}\delta_J^1 + \phi_{J,1}\delta_J^2) \end{Bmatrix} \\
&= \sum_{J=1}^{N} [B_J^u]\{\delta_J^u\} \ .
\end{aligned} \tag{7}$$

Similarly, we get

$$\nabla T = \begin{Bmatrix} T_{,1}(x_1, x_2) \\ T_{,2}(x_1, x_2) \end{Bmatrix} = \begin{Bmatrix} \sum_{J=1}^{N} \phi_{J,1}\delta_J^t \\ \sum_{J=1}^{N} \phi_{J,2}\delta_J^t \end{Bmatrix} = \sum_{J=1}^{N} [B_J^t]\{\delta_J^t\} \ . \tag{8}$$

Substitution from (6), (7) and (8) into $(2)_1$ and $(2)_2$, the result into (5), and requiring that the resulting equations hold for all choices of $\bar{\boldsymbol{\delta}}^u$ and $\bar{\boldsymbol{\delta}}^t$, we arrive at the following set of discrete equations.

$$\sum_{J=1}^{N} \mathbf{K}_{IJ}^u \boldsymbol{\delta}_J^u = \mathbf{F}_I^u, \quad \sum_{J=1}^{N} \mathbf{K}_{IJ}^t \boldsymbol{\delta}_J^t = \mathbf{F}_I^t \ , \tag{9}$$

where

$$\mathbf{K}^u_{IJ} = \int_{S_\alpha} (\bar{\mathbf{B}}^u_I)^{\mathrm{T}}\mathbf{D}\mathbf{B}^u_J \,\mathrm{d}A - \int_{\Gamma_{\alpha u}} (\psi^u_I)^{\mathrm{T}}\mathbf{n}\mathbf{D}\mathbf{B}^u_J \,\mathrm{d}\Gamma + \int_{\Gamma_{\alpha u}} \mathbf{p}_u\psi^u_I(\phi^u_J)^{\mathrm{T}} \,\mathrm{d}\Gamma,$$

$$\mathbf{K}^t_{IJ} = \int_{S_\alpha} (\bar{\mathbf{B}}^t_I)^{\mathrm{T}}\mathbf{D}^t\mathbf{B}^t_J \,\mathrm{d}A - \int_{\Gamma_{\alpha t}} \psi^T_I\mathbf{n}\mathbf{D}^t\mathbf{B}^t_J \,\mathrm{d}\Gamma + \int_{\Gamma_{\alpha t}} p_t\psi^t_I(\phi^t_I)^{\mathrm{T}} \,\mathrm{d}\Gamma,$$

$$\mathbf{F}^u_I = \int_{\Gamma_{\alpha f}} (\psi^u_I)^{\mathrm{T}}\bar{\mathbf{f}} \,\mathrm{d}\Gamma + \int_{\Gamma_{\alpha u}} p_u\psi^u_I\bar{\mathbf{u}} \,\mathrm{d}\Gamma + \int_{S_\alpha} (\bar{\mathbf{B}}^u_I)^{\mathrm{T}}\mathbf{C}\phi^t_J\boldsymbol{\delta}^t_J \,\mathrm{d}A - \int_{\Gamma_{\alpha u}} (\psi^u_I)^{\mathrm{T}}\mathbf{n}\mathbf{C}\phi^t_J\boldsymbol{\delta}^t_J \,\mathrm{d}\Gamma, \tag{10}$$

$$\mathbf{F}^t_I = \int_{\Gamma_{\alpha q}} (\psi^t_I)^{\mathrm{T}}\bar{\mathbf{q}} \,\mathrm{d}\Gamma + \int_{\Gamma_{\alpha t}} p_t\psi^t_I\bar{T} \,\mathrm{d}\Gamma \ .$$

Here

$$\mathbf{D} = \begin{bmatrix} \lambda+2\mu & \lambda & 0 \\ \lambda & \lambda+2\mu & 0 \\ 0 & 0 & \mu \end{bmatrix},$$

$$\mathbf{C} = \begin{Bmatrix} \beta \\ \beta \\ 0 \end{Bmatrix}, \quad \mathbf{D}^t = \begin{bmatrix} -\kappa & 0 \\ 0 & -\kappa \end{bmatrix} \ , \tag{11}$$

are respectively the matrices of elastic constants, stress–temperature coefficients and thermal conductivities. A superimposed bar denotes a quantity derived from the test functions $\mathbf{v}$ and θ corresponding to those for the trial solutions $\mathbf{u}$ and T. Equations (9) are written for each S_I, $1 \le I \le N$. There is no assembly of equations required in the MLPG method.

The basis functions $\{\phi^u_I\}$ and $\{\phi^t_I\}$ are found by the moving least squares (MLS) method of Lancaster and Salkauskas [19]; it is discussed below.

3.1 Brief description of the MLS basis functions

Let $f(x_1,x_2)$ be a scalar valued function defined on S_I; f can be identified with one of the three fields $u_1(x_1,x_2)$, $u_2(x_1,x_2)$ and $T(x_1,x_2)$. The approximation $f^h(x_1,x_2)$ of $f(x_1,x_2)$ is assumed to be given by

$$f^h(x_1,x_2) = \sum_{J=1}^{m} p_J(x_1,x_2)a_J(x_1,x_2) \ , \tag{12}$$

where

$$\mathbf{p}^{\mathrm{T}}(x_1,x_2) = \{1, x_1, x_2, (x_1)^2, x_1x_2, (x_2)^2, \ldots\} \ , \tag{13}$$

is a complete monomial in x_1 and x_2 having m terms. For example, $\mathbf{p}^{\mathrm{T}} = \{1, x_1, x_2\}$ with $m = 3$ and $\mathbf{p}^{\mathrm{T}} = \{1, x_1, x_2, (x_1)^2, x_1x_2, (x_2)^2\}$ with $m = 6$ are respectively complete monomials of degree 1 and 2. The coefficients $a_1(x_1,x_2)$, $a_2(x_1,x_2)$, …, $a_m(x_1,x_2)$ are found by minimizing R defined by

$$R(\mathbf{x}) = \sum_{I=1}^{n} W(\mathbf{x}-\mathbf{x}_I)[\mathbf{p}^{\mathrm{T}}(\mathbf{x}_I)\mathbf{a}(\mathbf{x}) - \hat{f}_I]^2 \ , \tag{14}$$

where $\hat{f}_I$ is the ficticious value of $f^h(\mathbf{x})$ at $\mathbf{x} = \mathbf{x}_I$, $\mathbf{x}_I$ gives the location of node I, and n is the number of nodes $(m \le n \le N)$ whose weight functions $W(\mathbf{x}-\mathbf{x}_I)$ have positive values at the point $\mathbf{x}$. Thus the weight function $W(\mathbf{x}-\mathbf{x}_I)$ is taken to be associated with the node I located at $\mathbf{x}_I$. Here we take

$$W(\mathbf{x}-\mathbf{x}_I) = \begin{cases} 1-6\left(\frac{d_I}{r_w}\right)^2+8\left(\frac{d_I}{r_w}\right)^3-3\left(\frac{d_I}{r_w}\right)^4, & 0 \le d_I \le r_w, \\ 0, & d_I > r_w \ , \end{cases} \tag{15}$$

where $d_I = |\mathbf{x}-\mathbf{x}_I|$ is the distance between points $\mathbf{x}$ and $\mathbf{x}_I$ and r_w is the radius of the circle outside which W vanishes. r_w is called the support of the weight function W.

Setting $\partial R/\partial a_I = 0$, $I = 1, 2, \ldots, m$ gives the following system of m linear algebraic equations for the determination of $a_1(\mathbf{x})$, $a_2(\mathbf{x})$, …, $a_m(\mathbf{x})$:

$$\mathbf{A}(\mathbf{x})\mathbf{a}(\mathbf{x}) = \mathbf{P}(\mathbf{x})\hat{\mathbf{f}} \ , \tag{16}$$

where

$$\mathbf{A}(\mathbf{x}) = \sum_{I=1}^{n} W(\mathbf{x}-\mathbf{x}_I)\mathbf{p}^{\mathrm{T}}(\mathbf{x}_I)\mathbf{p}(\mathbf{x}_I),$$
$$\mathbf{P}(\mathbf{x}) = [W(\mathbf{x}-\mathbf{x}_1)\mathbf{p}(\mathbf{x}_1),\ W(\mathbf{x}-\mathbf{x}_2)\mathbf{p}(\mathbf{x}_2), \ldots, W(\mathbf{x}-\mathbf{x}_n)\mathbf{p}(\mathbf{x}_n)] \ , \tag{17}$$

are $m \times m$ and $m \times n$ matrices. Note that elements of these matrices depend upon the choice of the weight functions. Solving equations (16) for $\mathbf{a}$ and substituting the result into (12) give

$$f^h(x_1,x_2) = \sum_{J=1}^{n} \phi_J(x_1,x_2)\hat{f}_J \ , \tag{18}$$

where

$$\phi_K(\mathbf{x}) = \sum_{J=1}^{m} p_J(\mathbf{x})[\mathbf{A}^{-1}(\mathbf{x})\mathbf{B}(\mathbf{x})]_{JK}, \quad K = 1, 2, \ldots, n \ , \tag{19}$$

are the basis functions of the MLS approximation. Note that $\phi_J(\mathbf{x}_K) \ne \delta_{JK}$; thus $\hat{f}_J \ne f^h(\mathbf{x}_J)$. For the matrix $\mathbf{A}$ to be invertible, $n \ge m$. Equation (18) gives the value of $f^h(\mathbf{x})$ in terms of the ficticious values $\hat{f}_J$ of $f^h(\mathbf{x})$ at n nodes whose weight functions are positive at the point $\mathbf{x}$. The value of n will vary with $\mathbf{x}$ and the radius, r_w, of the compact support of $W(\mathbf{x}-\mathbf{x}_I)$. Here we take

$$r_w = bh_I \quad , \tag{20}$$

where $h_I = \min\{|\mathbf{x}_J - \mathbf{x}_I|,\ 1 \le J \le N\}$ is the distance from the node at $\mathbf{x}_I$ to the node nearest to it and b is a scaling parameter.

3.2
Basis functions for the test function

The choice $\psi_I(\mathbf{x}) = \phi_I(\mathbf{x})$ in Eq. (6) will give a Galerkin formulation of the problem. However, it requires considerable computational resources to numerically evaluate integrals appearing in Eqs. (10). Here we take $\psi_I(\mathbf{x}) = W(\mathbf{x} - \mathbf{x}_I)$ with $r_w = h_I$. Taking S_I also equal to a circle of radius h_I centered at the node at $\mathbf{x}_I$ simplifies the evaluation of integrals appearing in Eqs. (10) and preserves the local character of the MLPG formulation. For S_I completely inside S, boundary or line integrals in Eqs. (10) identically vanish. When S_I intersects the boundary ∂S of S, then integrals in Eqs. (10) are evaluated on $S_I \cap S$ and the line integrals need not vanish.

3.3
Evaluation of integrals

For S_I a circle of radius h_I, the area integrals in Eqs. (10) are to be evaluated on a circle, and the line integrals on a part of the boundary of a circle. The circular region is mapped onto a $[-1,1] \times [-1,1]$ square region, and $N_g \times N_g$ Gauss integration points with the corresponding weights are used to numerically evaluate the integrals. In order to evaluate line integrals, the circular arc is mapped onto $[-1,1]$ and N_g Gauss points with the appropriate weights are used to evaluate the integrals.

3.4
Imposition of essential boundary conditions

Whereas the penalty method of satisfying essential boundary conditions works well for static problems, for dynamic problems it may significantly reduce the time step size [4]. Also a very large value of the penalty parameter can result in ill-conditioning of the stiffness matrices $\mathbf{K}^u$ and/or $\mathbf{K}^t$. If a displacement component (or temperature) is prescribed at a node, we replace equation $(9)_1$ for that node by an equation analogous to Eq. (18) with $u_i^h(x_1,x_2)$ (or $T^h(x_1,x_2)$) set equal to the prescribed value.

4
Estimation of effective elastic moduli

We assume that inclusions are spherical and are randomly distributed in the matrix. Furthermore both constituents are made of isotropic materials and the macroscopic response of the composite can be regarded as isotropic. Vel and Batra [43] have shown that the Mori–Tanaka [24] and the self-consistent [14] techniques give different results for a simply supported functionally graded plate loaded only on the top surface. The emphasis here is to demonstrate the applicability of the MLPG method to thermoelastic problems for inhomogeneous bodies. Thus the use of a particular homogenization technique for deducing effective properties of the composite is less critical. We use the Mori–Tanaka method for its simplicity. It accounts approximately for the interaction among neighboring inclusions and is generally applicable to regions of the graded microstructure that have a well-defined continuous matrix and a discontinuous particulate phase.

According to the Mori–Tanaka method, the effective shear modulus, μ, and the effective bulk modulus, K, of the two-phase composite are given by

$$\begin{aligned} \frac{K-K_1}{K_2-K_1} &= \frac{V_2}{1+(1-V_2)(K_2-K_1)/(3K_1+4\mu_1)}, \\ \frac{\mu-\mu_1}{\mu_2-\mu_1} &= V_2 \Big/ \left(1+(1-V_2)\frac{(\mu_2-\mu_1)}{(\mu_1+f_1)}\right) \quad , \end{aligned} \tag{21}$$

where

$$f_1 = \mu_1(9K_1+8\mu_1)/(6(K_1+2\mu_1)) \quad , \tag{22}$$

subscripts 1 and 2 denote quantities for phases 1 and 2 respectively, V_1 equals the volume fraction of phase 1, and $V_2 = 1 - V_1$ the volume fraction of phase 2. The Lamé constant λ is related to μ and K by $\lambda = K - 2\mu/3$. The effective thermal conductivity κ [13] and the effective coefficient of thermal expansion α [35] are given by

$$\frac{\kappa-\kappa_1}{\kappa_2-\kappa_1} = \frac{V_2}{1+(1-V_2)(\kappa_2-\kappa_1)/3\kappa_1} \quad , \tag{23}$$

$$\frac{\alpha-\alpha_1}{\alpha_2-\alpha_1} = \frac{1/K-1/K_1}{1/K_2-1/K_1} \quad . \tag{24}$$

The through-the-thickness variation of V_2 is assumed to be given by

$$V_2 = V_2^- + (V_2^+ - V_2^-)\left(\frac{1}{2}+\frac{x_2}{h}\right)^p \quad , \tag{25}$$

where superscripts + and − signify respectively values of the quantity on the top and the bottom surfaces of the plate, and the parameter p describes the variation of phase 2. $p = 0$ and ∞ correspond to uniform distributions of phase 2 with volume fractions V_2^+ and V_2^- respectively.

5
Computation and discussion of results

Because of the availability of analytical results [42], we analyse thermomechanical deformations of a simply supported Aluminum/Silicon Carbide (Al/SiC) rectangular plate and assign following values to various material and geometric parameters.

$$\begin{aligned} &L = 250\,\text{mm}, \quad h = 50\,\text{mm}, \quad T_0 = 0, \\ &b = 13, \quad M = 1207, \quad m = 3, \quad N_g = 9; \\ &\text{Al: } E_1 = 70\,\text{GPa}, \quad \nu_1 = 0.3, \\ &\alpha_1 = 23.4 \times 10^{-6}/K, \quad \kappa_1 = 233\,\text{W/m}\,K, \\ &\text{SiC: } E_2 = 427\,\text{GPa}, \quad \nu_2 = 0.17, \\ &\alpha_2 = 4.3 \times 10^{-6}/K, \quad \kappa_2 = 65\,\text{W/m}\,K \quad . \end{aligned} \tag{26}$$

That is, we use a uniform mesh of 1207 nodes with 71 nodes in the x_1-direction and 17 in the x_2-direction; see Fig. 2. Thus S_I is a circle of radius 2.94 mm. Eighty-one quadrature points are used to evaluate integrals over S_I.

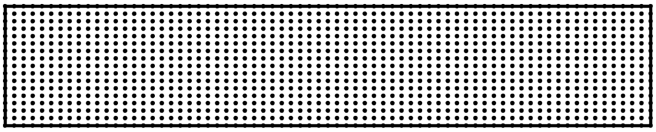

Fig. 2. Locations of 1207 uniformly distributed nodes on the cross section of the plate (nodes on the boundaries have been masked by the solid lines)

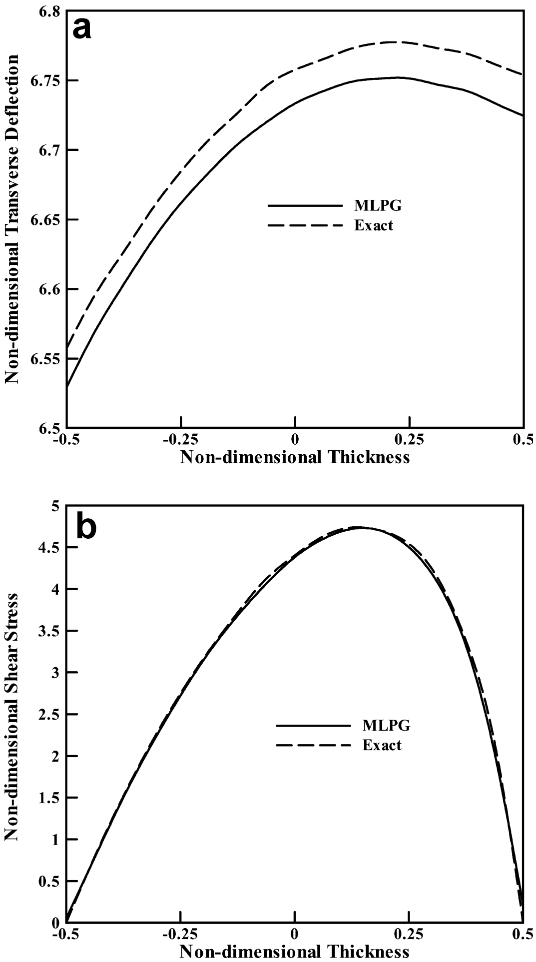

Fig. 3. For the pressure loading, comparison of through-the-thickness variation of **a** the transverse deflection and **b** the transverse shear stress at $x_1 = L/2$ computed by the MLPG method with the analytical solution of Vel and Batra [42]

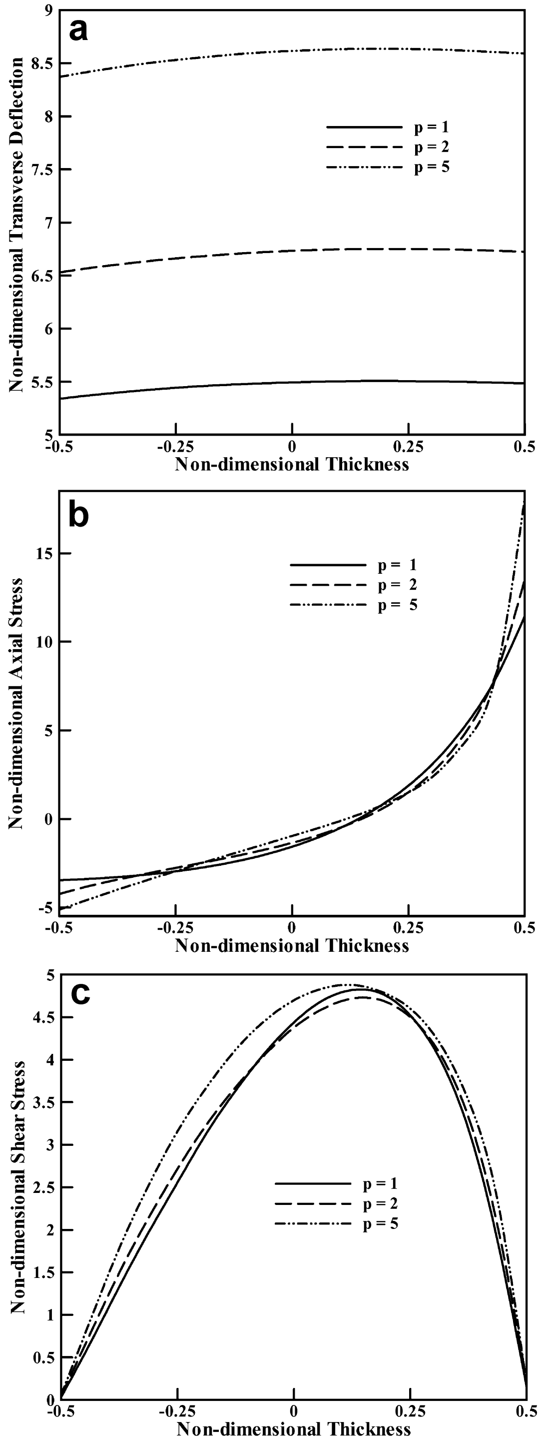

Fig. 4. Effect of the exponent p on the through-the-thickness variation of **a** the transverse deflection, **b** the axial stress, and **c** the transverse shear stress, on the section $x_1 = L/2$

The aspect ratio, L/h, equals 5 and the plate will be considered as being thick. In Eqs. (26), $E = 2\mu(1 + \nu)$ is Young's modulus and ν Poisson's ratio. Because a load (or temperature) prescribed on the surface $x_2 = h/2$ can be expanded in terms of Fourier series in x_1, it suffices to consider the following loads.

$$[\sigma_{22}(x_1,\ h/2),\ T(x_1,\ h/2)] = [p^+,\ T^+]\sin(\pi x_1/L),$$
$$\sigma_{12}(x_1,\ -h/2) = 0, \quad T(x_1,\ -h/2) = T_0\ . \tag{27}$$

Boundary conditions imposed at the simply supported edges are listed in Eq. $(4)_2$. Thus the two edges and the bottom surface of the plate are kept at a uniform temperature T_0. The top surface of the plate is subjected to a sinusoidal pressure load with amplitude p^+, and the thermal load on the top surface also varies sinusoidally with amplitude T^+. Either a mechanical or a thermal load is applied on the top surface of the plate. The problem for the combined loading can be solved by superposing solutions for the mechanical and the thermal problems.

For the mechanical load, results are presented in terms of the following non-dimensional variables

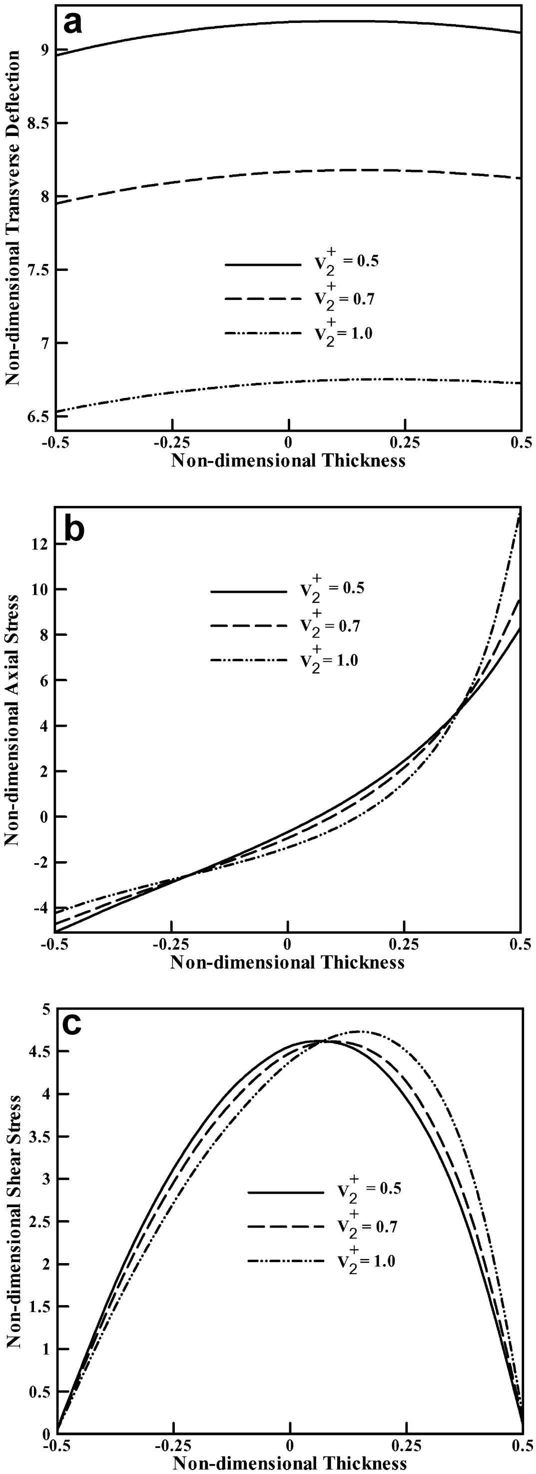

Fig. 5. Effect of V_2^+ (volume fraction of SiC at the top surface) on the through-the-thickness variation of **a** the transverse deflection, **b** the axial stress, and **c** the transverse shear stress, on the section $x_1 = L/2$

$$\bar{u}_2 = \frac{100 E_1 h^3 u_2}{p^+ L^4}, \quad \bar{\sigma}_{11} = \frac{10 h^2 \sigma_{11}}{p^+ L^2},$$
$$\bar{\sigma}_{12} = \frac{10 h \sigma_{12}}{p^+ L} \quad . \tag{28}$$

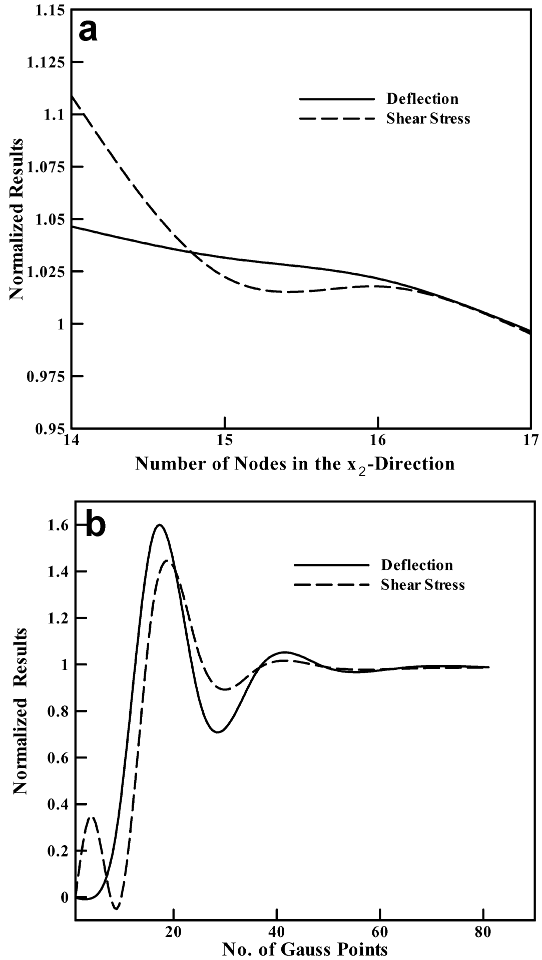

Fig. 6. Convergence of the deflection at the point $(L/2, 0)$ and the transverse shear stress at the point (0, 0) with the increase in the number of **a** nodes in the x_2-direction, and **b** Gauss points

For the thermal load, quantities are nondimensionalized as

$$\bar{u}_2 = \frac{100 h \ u_2}{\alpha_1 T^+ L^2}, \quad \bar{\sigma}_{11} = \frac{10 \sigma_{11}}{E_1 \alpha_1 T^+},$$
$$\bar{\sigma}_{12} = \frac{100 L \ \sigma_{12}}{E_1 \alpha_1 T^+ h} \quad . \tag{29}$$

Unless otherwise noted, we have set

$$V_2^- = 0, \quad V_2^+ = 1, \quad p = 2 \ , \tag{30}$$

in Eq. (25).

5.1 Results for the pressure load

Figures 3a and 3b respectively compare through-the-thickness variations of the transverse displacement, $\bar{u}_2$, and the transverse shear stress $\bar{\sigma}_{12}$ from the MLPG solution with those from the analytical solution of Vel and Batra [42]. Note the expanded vertical scale in Fig. 3a; thus small differences in the two values of $\bar{u}_2$ are exaggerated. The maximum difference in the two values of $\bar{u}_2$ is only 0.39%. The two values of the transverse shear stress essentially coincide with each other at every point in the plate. Thus the MLPG method yields accurate values of the displacements and stresses for a FG

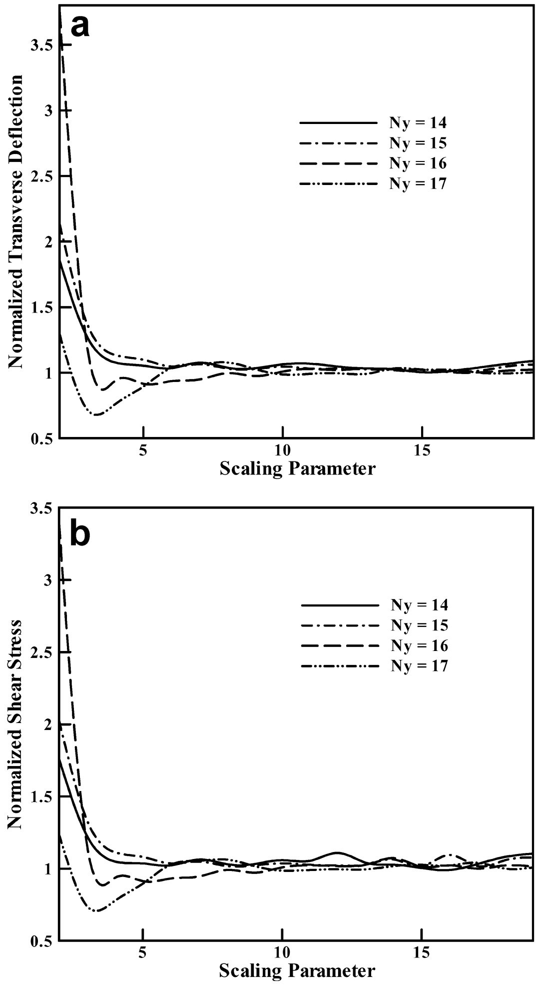

Fig. 7. Convergence of **a** the deflection at the point $(L/2, 0)$ and **b** the transverse shear stress at the point (0, 0) with the increase in the scaling parameter [N_y equals the number of uniformly spaced nodes in the x_2-direction]

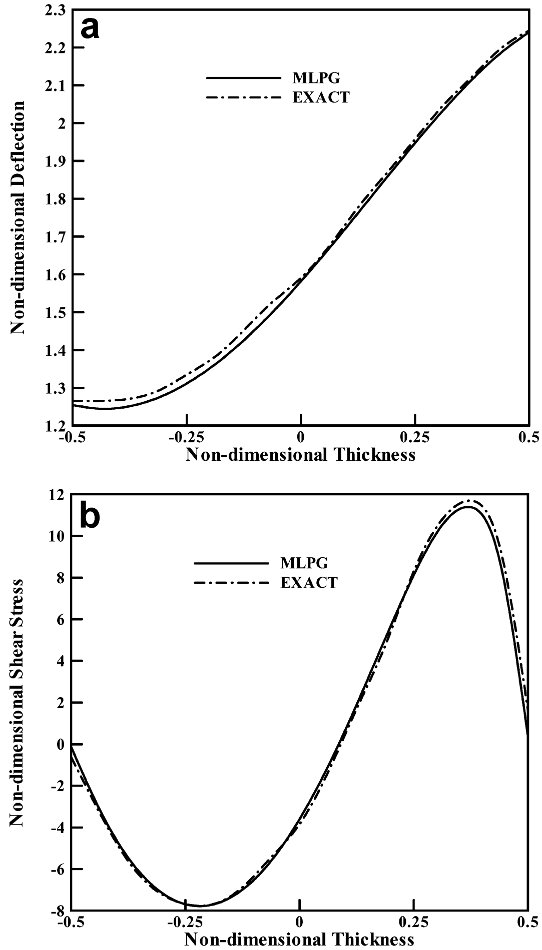

Fig. 8. For the thermal loading, comparison of through-the-thickness variation of **a** the transverse deflection and **b** the transverse shear stress at $x_1 = L/2$ mm computed by the MLPG method with the analytical solution of Vel and Batra [42]

plate. Note that the transverse deflection is not uniform through the plate thickness implying thereby the existence of the transverse normal strain. The transverse normal strain is positive for $x_2/h \leq 0.2$ and negative for $x_2/h > 0.2$. The maximum value of the transverse shear stress occurs at $x_2/h \simeq 0.15$. Figure 4a, b, c depicts the influence of the variation of the volume fraction of SiC on the through-the-thickness distribution of the transverse deflection, the axial stress, and the transverse shear stress. For fixed values of V_2^- and V_2^+, a higher value of p gives a lower value of V_2 and thus a lower value of the bending stiffness which in turn results in a higher value of the transverse deflection of the plate. The smooth slow variation of the transverse deflection implies that the transverse normal strain also changes gradually through the plate thickness. A higher value of p gives an increased value of the magnitude of the axial stress at points adjacent to the top and the bottom surfaces of the plate. As expected, the neutral surface does not pass through the horizontal centroidal axis of the plate. The axial stress on the top surface is considerably higher than the magnitude of the axial stress on the bottom surface. The maximum value of the transverse shear stress and where it occurs are not affected that much by the value of p.

Keeping $V_2^- = 0$ and $p = 2$ fixed, Fig. 5a, b, c shows the effect of varying V_2^+ on the through-the-thickness variations of the transverse deflection, the axial stress, and the transverse shear stress. The qualitative nature of results is unaffected by the value of V_2^+; however, a higher value of V_2^+ gives lower deflection of points on the top and the bottom surfaces, a higher value of the axial stress at points on the top surface, and a slightly higher value of the maximum transverse shear stress. The point where the maximum transverse shear stress occurs moves towards the top surface with an increase in the value of V_2^+.

5.2
Variation of parameters of the MLPG method

We have plotted in Fig. 6a the variation of the transverse deflection at the point $(L/2, 0)$ and the transverse shear stress at the point (0, 0) with the number of nodes in the x_2-direction. The ordinate equals the value of a quantity normalized by its value for the 17 node case. It is clear that we need a minimum of 16 uniformly spaced nodes in the x_2-direction. For a homogeneous cantilever beam loaded

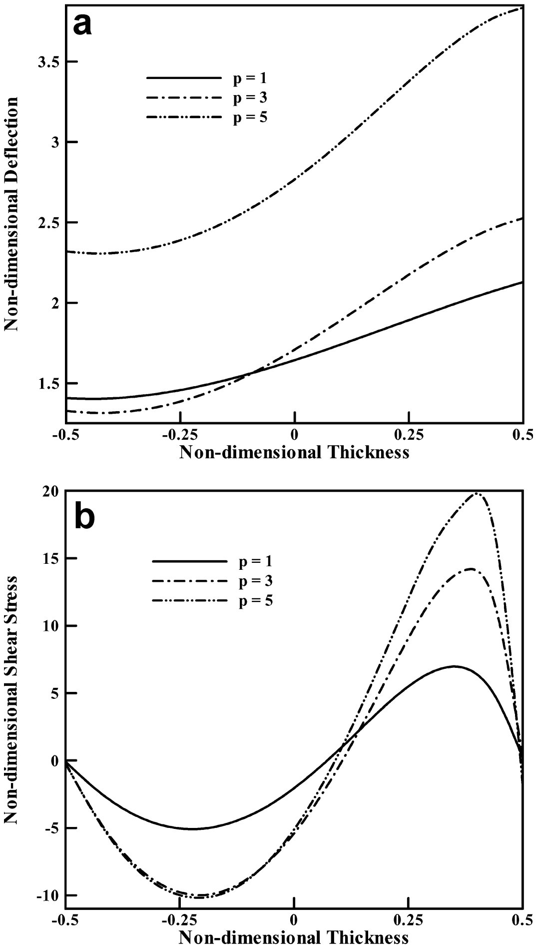

Fig. 9. Effect of the exponent p on the through-the-thickness variation of **a** the transverse deflection, and **b** the transverse shear stress on the section $x_1 = 125\,\mathrm{mm}$

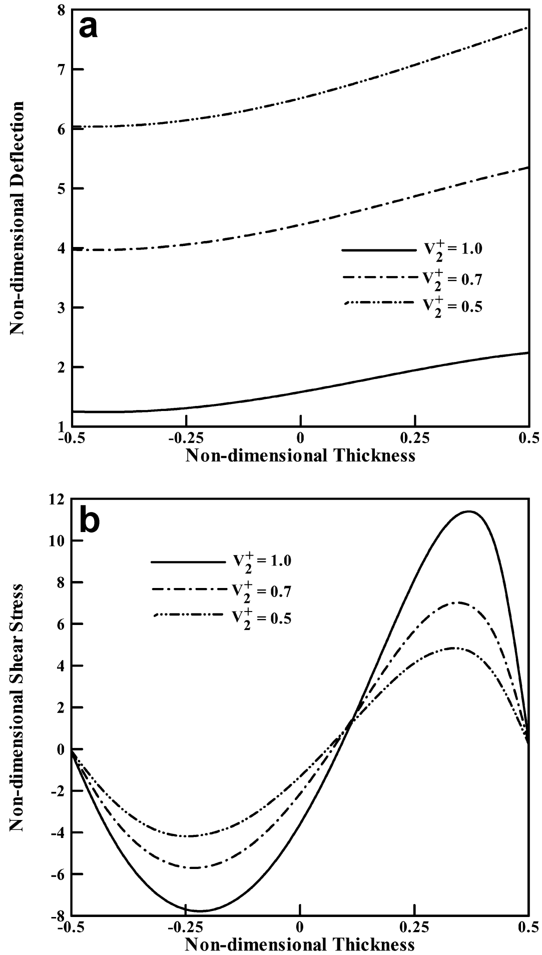

Fig. 10. Effect of V_2^+ (volume fraction of SiC at the top surface) on the through-the-thickness variation of **a** the transverse deflection, and **b** the transverse shear stress on the section $x_1 = L/2\,\mathrm{mm}$

on the unclamped edge by a tangential force, 72 uniformly spaced nodes with 4 nodes in the thickness direction gave a solution that matched the analytical solution of the problem (Ching [8]). Results plotted in Fig. 6b reveal that a 7×7 Gauss quadrature rule would have been sufficient. Figure 7a, b exhibits the influence of the scaling parameter b defined in Eq. (20) on the transverse deflection and the transverse shear stress; N_y equals the number of nodes in the x_2-direction. Irrespective of the value of N_y in the range of 14 to 17, $b \geq 8$ should give acceptable results.

5.3
Results for the thermal load

We have compared in Fig. 8a, b the computed transverse deflection and the transverse shear stress with the analytical solution of Vel and Batra [42]. As for the pressure loading, the MLPG solution matches very well with the analytical solution. Whereas for the pressure load applied only on the top surface of the plate, the maximum deflection occurs at the point $x_2/h = 0.2$, for the thermal loading the transverse deflection monotonically increases with x_2 in the range $-0.25 \leq x_2/h \leq 0.5$. Thus the transverse normal strain is positive at most points in the transverse direction. The through-the-thickness variation of the transverse shear stress consists of two half sine waves of different amplitudes and wavelengths. Results plotted in Fig. 9a, b exhibit that the qualitative variation of the through-the-thickness nature of the transverse deflection and the transverse shear stress is unaffected by the value assigned to the exponent p giving the change in the volume fraction of SiC. For a given thermal loading, results plotted in Figs. 9 and 10 evince that the transverse deflection of a point on the top surface increases with an increase in the value of p or a decrease in the value of V_2^+, and the maximum transverse shear stress increases with an increase in the value of p and/or V_2^+.

6
Conclusions

We have extended the meshless local Petrov–Galerkin (MLPG) formulation to analyse static thermomechanical deformations of a thick functionally graded thermoelastic plate. The effective properties at a point in the plate are obtained by the Mori–Tanaka method. The volume fraction of the two constituents, and hence the effective moduli are assumed to vary only in the thickness direction. Streses and displacements computed with the MLPG method are found to agree very well with those obtained from the analytical solution of the corresponding problems. The number of uniformly spaced nodes in the direction of variation of material properties is significantly more than that needed to analyze deformations of a similarly loaded homogeneous thick plate. For several variations of the material properties, seventeen nodes in the thickness direction and a 7×7 quadrature rule for evaluating integrals over local circular subdomains yielded stresses and displacements in close agreement with their analytical values. An advantage of the MLPG method is that neither nodal connectivity nor a background mesh is needed for solving numerically a boundary-value problem. The collocation method, the finite-difference method and the smoothed-particle hydrodynamics also do not require a background mesh. These methods employ the strong form of a boundary-value problem and the MLPG method uses a weak form.

References

1. **Aboudi J, Pindera M-J, Arnold SM** (1995) A coupled higher-order theory for functionally graded composites with partial homogenization. Comput. Eng. 5: 771–792
2. **Atluri SN, Zhu T** (1998) A new meshless local Petrov–Galerkin (MLPG) approach in computational mechanics. Comput. Mech. 22: 117–127
3. **Atluri SN, Shen SP** (2002) The Meshless Local Petrov-Galerkin (MLPG) Method. Tech. Sci. Press
4. **Batra RC, Ching HK** (2002) Analysis of elastodynamic deformations near a crack notch tip by the meshless local Petrov–Galerkin (MLPG) method. Comput. Model. Eng. Sci. 3: 717–730
5. **Batra RC, Porfiri M, Spinello, D** (2003) Treatment of material discontinuity in two meshless local Petrov–Galerkin (MLPG) formulations of axisymmetric transient heat conduction. submitted for publication
6. **Belytschko T, Lu YY, Gu L** (1994) Element-free Galerkin methods. Int. J. Numer. Methd. Eng. 37: 229–256
7. **Cheng ZQ, Batra RC** (2000) Three-dimensional thermoelastic deformations of a functionally graded elliptic plate. Composites: Part B 31: 97–106
8. **Ching HK** (2002) Solution of Linear Elastostatic and Elastodynamic Plane Problems by the Meshless Local Petrov–Galerkin Method. Ph.D. dissertation, Virginia Polytechnic Institute and State University, Blacksburg, VA
9. **Ching HK, Batra RC** (2001) Determination of crack tip fields in linear elastostatics by the meshless local Petrov–Galerkin (MLPG) method. Comput. Model. Eng. Sci. 2(2): 273–289
10. **Duarte CA, Oden JT** (2000) H-p clouds – an *hp* meshless method. Numer. Meth. Partial Differential Equations 1–34
11. **Fröhlich H, Sack R** (1946) Theory of the rheological properties of dispersions. Proc. Roy. Soc. A 185: 415–430
12. **Gu YT, Liu GR** (2001) A meshless local Petrov–Galerkin (MLPG) method for free and forced vibration analyses for solids. Comput. Mech. 27: 188–198
13. **Hatta H, Taya M** (1985) Effective thermal conductivity of a misoriented short fiber composite. J. Appl. Phys. 58(7): 2478–2486
14. **Hill R** (1965) A self-consistent mechanics of composite materials. J. Mech. Phys. Solids 13: 213–222
15. **Hirano T, Teraki J, Yamada T** (1990) Application of fuzzy theory to the design of functionally gradient materials. SMIRT 11 Transact. SD1 49–54
16. **Jiang B, Batra RC** (2002) Effective properties of a piezocomposite containing shape memory alloy and inert inclusions. Contin. Mech. Thermody. 14: 87–111
17. **Jin ZH, Batra RC** (1996) Stress intensity relaxation at the tip of an edge crack in a functionally graded material subjected to a thermal shock. J. Thermal Stresses 19: 317–339
18. **Krongauz Y, Belytschko T** (1989) EFG approximation with discontinuous derivatives. Int. J. Numer. Meth. Eng. 41: 1215–1233
19. **Lancaster P, Salkauskas K** (1981) Surfaces generated by moving least squares methods. Math. Comput. 37: 141–158
20. **Liu GR** (2003) Mesh Free Methods. CRC Press, Boca Raton
21. **Liu W, Jun S, Zhang Y** (1995) Reproducing kernel particle method. Int. J. Numer. Meth. Eng. 20: 1081–1106
22. **Lucy LB** (1977) A numerical approach to the testing of the fission hypothesis. Astronomical J. 82(12): 1012–1024
23. **Melenk JM, Babuska I** (1996) The partition of unity finite element method: Basic theory and applications. Comput. Meth. Appl. Mech. Eng. 139: 289–314
24. **Mori T, Tanaka K** (1973) Average stress in matrix and average elastic energy of materials with misfitting inclusions. Acta Metallurgica 21: 571–574
25. **Nagase Y, Ichikawa Y, Kirigai A, Amada S, Munekata T, Ahifei Y** (1996) The mechanical structures of bamboo in viewpoint of functionally gradient and composite materials. J. Comput. Mater. 30: 800–819
26. **Nayroles B, Touzot G, Villon P** (1992) Generalizing the finite element method: diffuse approximation and diffuse elements. Comput. Mech. 20: 307–318
27. **Organ DJ, Fleming M, Belytschko T** (1996) Continuous meshless approximations for nonconvex bodies by diffraction and transparency. Comput. Mech. 18: 225–235
28. **Okano K, Takagi Y** (1996) Application of SiC–Si functionally gradient material to thermoelectric energy conversion device. Elect. Eng. Japan 117: 9–17
29. **Qian LF, Batra RC, Chen LM** (2003) Elastostatic deformations of a thick plate by using a higher-order shear and normal deformable plate theory and two meshless local Petrov–Galerkin (MLPG) methods. Comput. Model. Eng. Sci. 4: 161–176
30. **Qian LF, Batra RC, Chen LM** (2003) Free and forced vibrations of thick rectangular plates by using higher-order shear and normal deformable plate theory and meshless local Petrov–Galerkin (MLPG) method. Comput. Model. Eng. Sci. 4: 519–534
31. **Qian LF, Batra RC, Chen LM** (2003) Static and dynamic deformations of thick functionally graded elastic plate by using higher-order shear and normal deformable plate theory and meshless local Petrov–Galerkin method. Composites: Part B (accepted)
32. **Qian LF, Batra RC** (2003) Three-dimensional transient heat conduction in a functionally graded thick plate with a higher-order plate theory and a meshless local Petrov–Galerkin method. submitted for publication
33. **Qian LF, Batra RC** (2003) Transient thermoelastic deformations of a thick functionally graded plate. submitted for publication
34. **Rogers TG, Watson P, Spencer AJM** (1995) Exact three-dimensional elasticity solutions for bending of moderately thick inhomogeneous and laminated strips under normal pressure. Int. J. Solids Struct. 32(12): 1659–1673
35. **Rosen BW, Hashin Z** (1970) Effective thermal expansion coefficients and specific heats of composite materials. Int. J. Eng. Sci. 8: 157–173
36. **Satyamurthy K, Hasselman DPH, Singh JP, Kamat MP** (1980) Effect of spatial variation of thermal conductivity on magnitude of tensile thermal stress in brittle materials subjected to convective heating. In: Hasselman DPH, Heller RA (eds) Thermal Stresses in Severe Environments, Plenum Press, New York pp. 325–342
37. **Sukumar N, Moran B, Belytschko T** (1998) The natural element method in solid mechanics. Int. J. Numer. Meth. Eng. 43: 839–887
38. **Tarn JQ, Wang YM** (1995) Asymptotic thermoelastic analysis of anisotropic inhomogeneous and laminated plates. J. Thermal Stresses 18(1): 35–58

39. **Uchimoto Y, Inaba M, Tasaka A, Komura A, Ogumi Z** (1996) Preparation of functionally gradient fluorocarbon polymer films by plasma polymerization of NF3 and propylene. J. Polymer Sci. Part A-Poly. Chem. 34(2): 193–198
40. **Vel SS, Batra RC** (2003) Three-dimensional analysis of transient thermal stresses in functionally graded plates. Int. J. Solids Struct. 40, 7181–7196
41. **Vel SS, Batra RC** (2003) Three-dimensional exact solution for the vibration of functionally graded rectangular plates. J. Sound Vibration (in press)
42. **Vel SS, Batra RC** (2003) Exact thermoelasticity solution for cylindrical bending vibrations of functionally graded plates. In: Watanabe K, Ziegler F (eds) Proc. IUTAM Symp. on Dynamics of Advanced Materials and Smart Structures. Kluwer Academic Publishers, Dordrecht, Boston, London
43. **Vel SS, Batra RC** (2002) Exact solution for thermoelastic deformations of functionally graded thick rectangular plates. AIAA J. 40: 1421–1433
44. **Ward E, Jones J, Jones R, Shnitser P, Kukhtarev N, Kukhtareva T** (2000) New concept of transient functionally graded material for thermoelectric power conversion. In: Proceedings of SPIE-The International Society for Optical Engineering. Bellingham, WA 4042: 146–155
45. **Wendland H** (1995) Piecewise polynomial, positive definite and compactly supported radial basis functions of minimal degree. Adv. Comput. Meth. 4: 389–396
46. **Batra RC, Vidoli S** (2002) Higher order piezoelectric plate theory derived from a three-dimensional variational principle. AIAA J. 40(1): 91–104